

DCA for the $2D$ Hubbard model at $T \rightarrow 0$

Th. Pruschke¹, R. Zitzler², Th.A. Maier³ and M. Jarrell⁴

¹ Institute for Theoretical Physics, University of Göttingen, Tammanstr. 1, 37077 Göttingen, Germany

² Center for electronic correlations and magnetism, Theoretical Physics III, Institute for Physics, University of Augsburg, 86135 Augsburg, Germany

³ Computer Science and Mathematics Division, Oak Ridge National Laboratory, Oak Ridge, TN 37831-6164, USA

⁴ Department of Physics, University of Cincinnati, Cincinnati OH 45221, USA

Summary. We discuss single particle dynamics of the half-filled $2D$ Hubbard model at $T \rightarrow 0$ calculated within the dynamical cluster approximation, using NRG as non-perturbative cluster solver, which requires the use parallel architectures with large number of processors and memory. In addition, fast temporal storage for out-of-core matrices is needed. The results obtained indicate that the half-filled $2D$ Hubbard model at $T \rightarrow 0$ is a paramagnetic insulator for *all* values of the Coulomb interaction U in strong contrast to weak-coupling theories.

Introduction

The microscopic description of magnetism and metal-insulator transitions constitutes one of the major research activities in modern solid state theory. Especially transition metal compounds like V_2O_3 , $LaTiO_3$, $NiS_{2-x}Se_x$ and the cuprates show metal-insulator transitions and magnetic order depending on composition, pressure or other control parameters [1]. The paramagnetic insulating phase observed in these materials is believed to be a so-called Mott-Hubbard insulator due to electron-electron correlations; in contrast to Slater or band insulators like $SrTiO_3$.

The simplest model showing both magnetism and a correlation-induced metal-insulator transition (MIT) is the one-band Hubbard model [2]

$$H = - \sum_{i,j,\sigma} t_{ij} c_{i\sigma}^\dagger c_{j\sigma} + \frac{U}{2} \sum_{i\sigma} n_{i\sigma} n_{i\bar{\sigma}} . \quad (1)$$

Considerable progress in understanding the physics of this simple but nevertheless non-trivial model has been achieved in the last decade through the development of the dynamical mean-field theory (DMFT) [3–5]. In particular, the phase diagram for the unfrustrated Hubbard model is very well understood [4,5]. At half-filling the physics is dominated by an antiferromagnetic insulating phase (AFI) for all $U > 0$ with a maximum $T_N \approx 0.15W$ around $U \approx W$, where W is the bandwidth of the non-interacting system.

For finite doping, the antiferromagnetic phase persists up to a critical doping δ_c [6] and in addition shows phase separation [7, 8]. For very large values of U the antiferromagnetic phase is replaced by a small region of Nagaoka type ferromagnetism [9–11].

Beyond this mean-field description, the situation is less clear. Except for spatial dimension $D = 1$, where it has been proven rigorously that the system at half filling is a paramagnetic insulator for all $U > 0$ [12], the question to what extent the paramagnetic Mott-Hubbard metal-insulator transition is a generic effect has not been addressed satisfactorily.

Since phenomena like the Mott-Hubbard transition are intrinsically non-perturbative in nature, we use the recently developed dynamical cluster approximation (DCA) [13–17] to study the low-energy behavior of the $2D$ Hubbard model at half filling in the weak to intermediate coupling regime. The DCA systematically incorporates non-local corrections to local approximations like the dynamical mean field, by mapping the lattice onto a self-consistently embedded cluster. We solve the cluster problem using for the first time Wilson’s numerical renormalization group (NRG) technique [18]. With this technique we are able to produce non-perturbative results in the thermodynamic limit at $T \rightarrow 0$, which is necessary to unambiguously identify the Mott-Hubbard transition in the dynamics [19].

The paper is organized as follows. The next section contains a brief introduction to the DCA. The numerical results will be presented in the third section followed by a discussion and summary.

Formalism

Theoretical background

A detailed discussion of the DCA formalism was already given in a previous publication [20]. The main assumption underlying the DCA is that the single-particle self-energy $\Sigma(\mathbf{k}, z)$ is a slowly varying function of the momentum \mathbf{k} and can be approximated by a constant within each of a set of cells centered at a corresponding set of momenta \mathbf{K} in the first Brillouin zone [13]. Within this approximation, one can set up a self-consistency cycle similar to the one in the dynamical mean-field theory (DMFT) [4, 5]. However, in contrast to the DMFT, where only local correlations are taken into account, the DCA includes non-local dynamical correlations. The length scales of these non-local correlations can be varied systematically from short ranged to long ranged by increasing the number of coarse-graining cells. The DCA collapses to the DMFT if one represents the Brillouin zone by one cell only, thus setting the characteristic length scale to zero.

For the impurity problem of the DMFT a large set of reliable numerical techniques has been developed over the past ten years [4, 5, 21, 22]. In par-

ticular, for $T = 0$ and low temperatures, the NRG has turned out to be the method of choice [8, 19].

The NRG introduces a logarithmic discretization of the energy axis, which allows a mapping of the cluster Hamiltonian to a set of semi-infinite chains coupled to the cluster degrees of freedom at their left end. The important aspect is that, within each chain, a coupling exists between nearest neighbors only and decreases exponentially with increasing chain size (for details see e.g. [18]). Thus, adding a new site to a chain with given length N will mix only states in a restricted energy window. This observation is then used to set up the following algorithm, which is visualised in Fig. 1:

- (i) Diagonalize the system with chains with N sites
- (ii) Keep only a handable number of eigenstates above the ground state
- (iii) Using this restricted space, generate the Hamilton matrix for the system with $N + 1$ sites
- (iv) Continue with step 1. until desired accuracy has been reached

Finally, calculate the desired physical quantities and proceed with the DCA self-consistency. As becomes apparent from the schematic view in Fig.1 this procedure prevents the exponential increase of the dimension of the matrices with increasing system size. The price one pays is the loss of information at higher energies. However, this can be partially compensated by keeping the information about physical quantities from chains with less sites [18].

Computational requirements

In principle the NRG algorithm does not suffer from an exponential increase of the size of the matrices to diagonalize, and its application to the DMFT [8, 19] requires only standard workstation resources. However, the extension to complex problems like the DCA still increases the demand in computational power drastically. While for a single impurity each chain site increases the Hilbert space by a factor 4, this factor becomes 4^{N_c} for a DCA calculation with N_c cluster sites. Thus, for the time being, the code is limited to a cluster size $N_c = 2$. To improve the performance and efficiency of the code in particular for larger cluster sizes, it is currently extended to use the distributed array implementations of ScaLAPACK and GlobalArray. With this technique we believe that at least $N_c = 4$ will be accessible in the near future.

For the results with $N_c = 2$ presented here, the typical memory consumption was roughly 4GB and in addition to distributed parallelism using MPI a hand-implemented SMP parallelism on the basis of POSIX threads was necessary to obtain decent computation times [23]. This code leads to an almost linear speed-up for up to 8 SMP processors in the application discussed here (see Fig. 2). The code was run on the Hitach SR8000 and the IBM Regatta at the computer center of the Max-Planck society at Garching. For the diagonalization the LAPACK routine DSYEV was used, while the standard

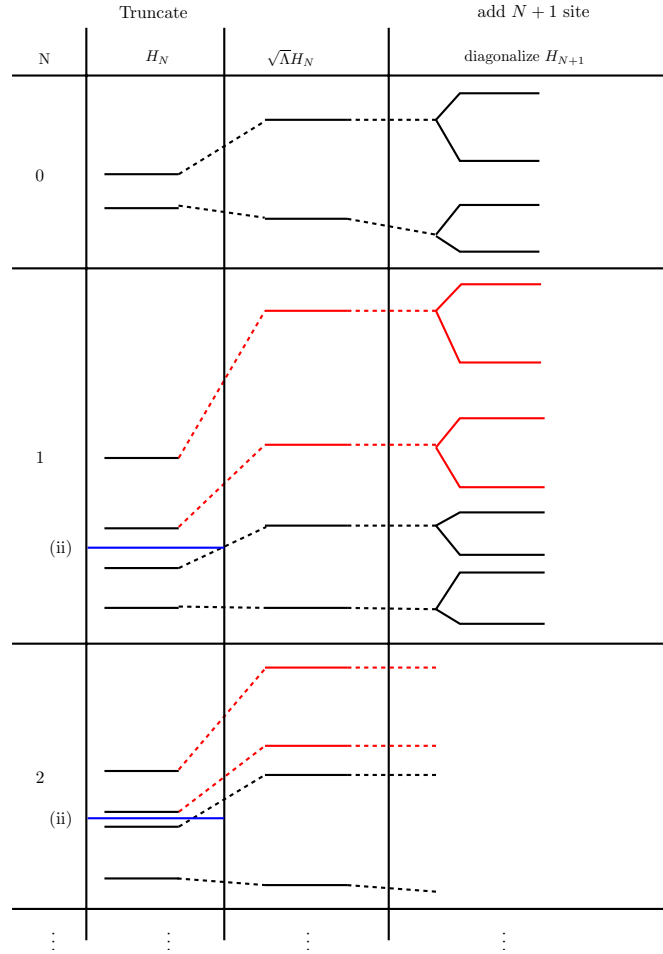


Fig. 1. Schematic view of the NRG algorithm. The blue lines marked (ii) represent the truncation step. In the construction of H_{N+1} , levels above these lines (drawn in red) will be omitted and the size of the Hamilton matrix to diagonalize is always 4×4 .

linear algebra operations were done with BLAS routines. The resulting performance was on the order of 0.8Gflop/s for the Hitachi and 3...3.5Gflop/s for the Regatta and a typical production run (i.e. one NRG run as part of about 10 DCA iterations) consumed roughly 24h total CPU time.

In addition to the in-core matrices, a matrix class with out-of-core structure was developed to prevent an inflation of allocated memory from the structures holding informations about physical quantities. This technique requires additional fast local I/O and temporary space on the order of 10–50

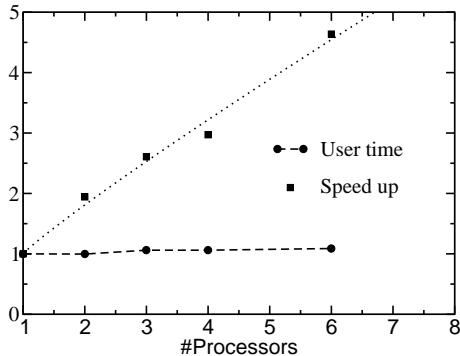


Fig. 2. Total user time and speed-up of the NRG code with POSIX threading as function of number of SMP processors. The user time is scaled with its value for one processor (≈ 12 h on the IBM Regatta at the RZ Garching).

GB. For such an application both the Hitachi and the Regatta provide an excellent environment.

Since the NRG is applied to such a complex problem for the first time here, Quantum Monte-Carlo (QMC) calculations for large clusters and finite temperatures (see e.g. [20] for performance details) were performed in addition to validate the NRG results.

Only due to this performance on modern massively parallel computer systems the application of the DCA with QMC or NRG to physical problems is possible at all.

Results

In the following we will discuss our NRG results for a DCA calculation with $N_c = 2$. While this cluster size seems, at first sight, too small to draw any reliable conclusions, recent publications [24–26] support that it already contains all essential ingredients to properly describe at least the qualitative effects of nonlocal correlations. In addition, the results presented here are the first calculations at $T = 0$ for an embedded cluster theory based on a non-perturbative technique.

The simplest realization of the Hubbard model (1) in $D = 2$ is a square lattice with nearest-neighbor hopping. In this case, the dispersion has the form

$$\varepsilon_{\mathbf{k}} = -2t (\cos(k_x) + \cos(k_y)) \quad . \quad (2)$$

In the following, we use $t = 1$ as our energy scale, i.e. the bandwidth of the dispersion (2) is $W = 8$. The proper tiling of the first Brillouin zone is shown in Fig. 3. The two \mathbf{K} vectors are located at $\mathbf{K}_0 = (0, 0)$ and $\mathbf{K}_\pi = (\pi, \pi)$ with corresponding cells labeled M_0 and M_π , respectively. The “coarse graining”

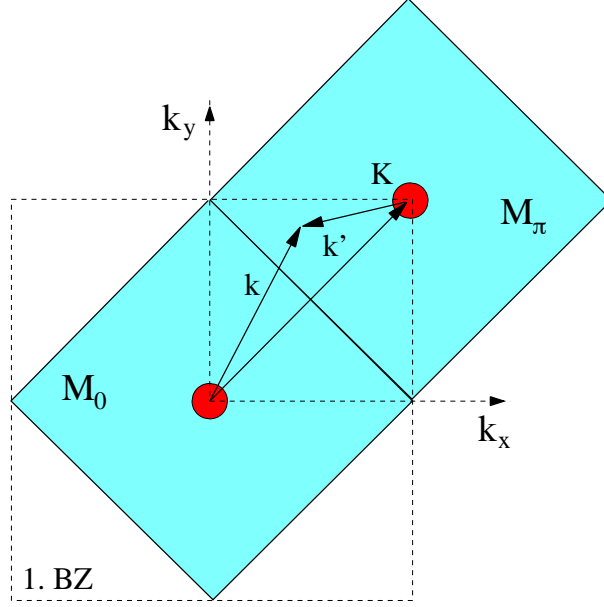


Fig. 3. Tiling of the first Brillouin zone for $N_c = 2$. M_0 and M_π label the sets of \mathbf{k} vectors belonging to $\mathbf{K}_0 = (0, 0)$ and $\mathbf{K}_\pi = (\pi, \pi)$, respectively.

necessary to define the effective cluster propagators then leads to the following quantities

$$\begin{aligned}\bar{G}(\mathbf{K}_0, z) &= \frac{2}{N} \sum_{\mathbf{k}' \in M_0} \frac{1}{z + \mu - \varepsilon_{\mathbf{K}_0 + \mathbf{k}'} - \Sigma(\mathbf{K}_0, z)} \\ \bar{G}(\mathbf{K}_\pi, z) &= \frac{2}{N} \sum_{\mathbf{k}' \in M_\pi} \frac{1}{z + \mu - \varepsilon_{\mathbf{K}_\pi + \mathbf{k}'} - \Sigma(\mathbf{K}_\pi, z)}\end{aligned}\quad (3)$$

The special form of the dispersion (2) allows for a conversion of the expressions (3) into energy integrals

$$\begin{aligned}\bar{G}(\mathbf{K}_0, z) &= 2 \int_0^\infty d\varepsilon \rho^{(0)}(\varepsilon) \frac{1}{z + \mu + \varepsilon - \Sigma(\mathbf{K}_0, z)} \\ \bar{G}(\mathbf{K}_\pi, z) &= 2 \int_0^\infty d\varepsilon \rho^{(0)}(\varepsilon) \frac{1}{z + \mu - \varepsilon - \Sigma(\mathbf{K}_\pi, z)} \\ \rho^{(0)}(\varepsilon) &= \frac{2}{\pi^2} \text{K} \left(\sqrt{1 - \left(\frac{\varepsilon}{4}\right)^2} \right)\end{aligned}\quad (4)$$

with $\text{K}(x)$ the complete elliptical integral of the first kind.

For $U = 0$, the self energies in (4) are identically zero and the resulting spectral functions defined as $A(\mathbf{K}, \omega) = -\frac{1}{\pi} \Im m G(\mathbf{K}, \omega + i0^+)$ are shown in Fig. 4. From weak-coupling theory [27] one expects no dramatic renormal-

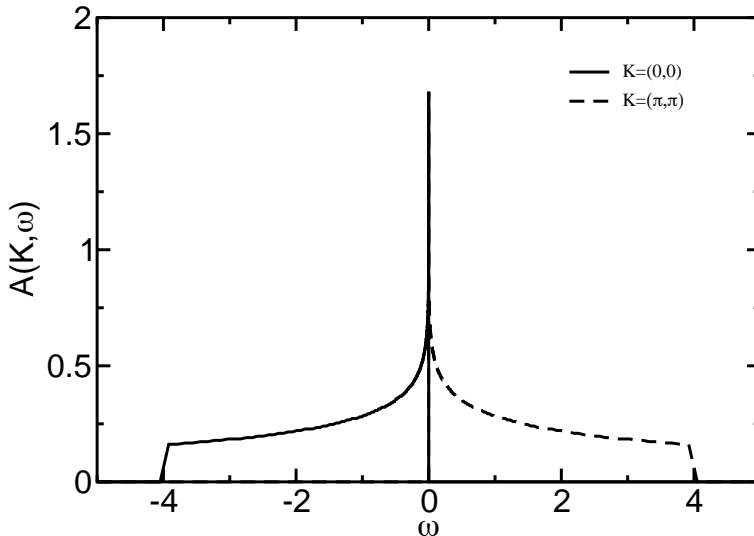


Fig. 4. Spectral functions for $U = 0$. Note the characteristic logarithmic van Hove singularity at the chemical potential $\omega = 0$.

ization of these structures at small values of U [28]. Only if one allows for antiferromagnetic ordering, a gap will open, leading to a so-called Slater insulator. Since such a magnetic ordering will always be present in finite size calculations like exact diagonalization or QMC [26, 29], it is impossible to extract informations about the structure of the one-particle excitations in the paramagnetic phase from these calculations, except for high temperatures. One interesting feature of the DCA however is that it allows to artificially suppress the magnetic ordering even in the ground state and thus enables one to extract informations about the development of the dynamics in the paramagnetic state in the limit $T \rightarrow 0$. The results of this calculation with the NRG for three different values $U = t = \frac{1}{8}W$, $U = 6t = \frac{3}{4}W$ and $U = 16t = 2W$ of the Coulomb parameter are shown in Fig. 5. Most notably, a gap opens at the Fermi surface independent of the value of U . Since no long range antiferromagnetic order is present, which would naturally lead to such a gap due to the reduced translational symmetry, this gap has to be attributed to strong short-ranged correlations present in the system even for infinitesimally small U .

Another interesting quantity is the momentum distribution function $n_{\mathbf{k}}$. For a conventional Fermi liquid, this function shows a jump at the Fermi

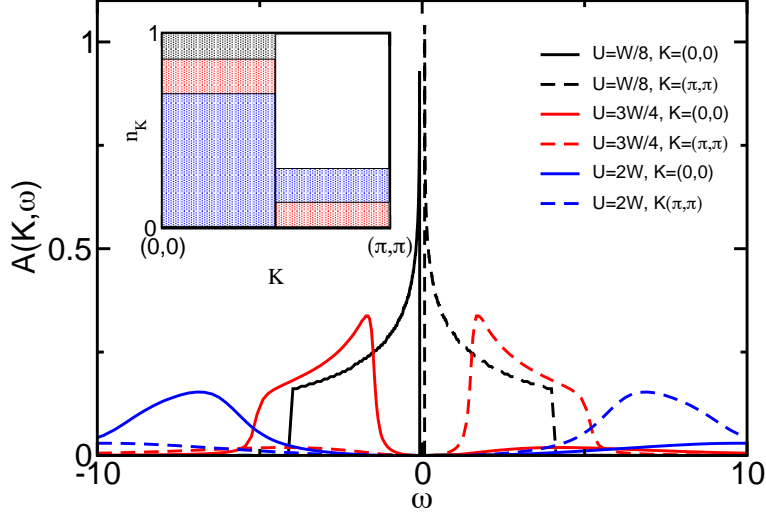


Fig. 5. Spectral functions for $U = t$, $U = 6t$ and $U = 16t$. For all three values there is a finite gap at the Fermi energy. The inset shows the coarse grained momentum distribution $n_{\mathbf{K}}$. The color coding is the same as in the main panel. Note that for large U n_0 and n_{π} come closer, a typical sign for localization in real space.

wave vector, while a Mott insulator should exhibit a constant $n_{\mathbf{k}} = 0.5$, i.e. the electronic states are completely localized in real space. Of course, from two \mathbf{K} points it is impossible to infer whether there is a jump at the Fermi wave vector or not. However, certain trends can be seen and interpreted. The inset to Fig. 5 shows the coarse grained $n_{\mathbf{K}}$ with the same color coding as in the main panel. Note that for very small U the momentum distribution looks like that of the system at $U = 0$. However, with increasing U , weight is shifted into the region above the Fermi surface of the noninteracting system, eventually leading to $n_0 \approx n_{\pi} \approx 1/2$, i.e. the distribution characteristic for the Mott insulator. Thus, while the system is insulating for all $U > 0$, the character of the electronic degrees of freedom seems to change nevertheless with increasing U , eventually leading to a Mott insulator at large enough U . Whether this will be a smooth crossover or possibly a transition can of course not be inferred from these results. However, recent investigations of the antiferromagnetic state in the DMFT suggest that one rather should expect a smooth crossover [32].

One might of course suspect that this behavior is an artefact of the small cluster size of $N_c = 2$ used here. That this is not the case can be inferred from DCA calculations for larger clusters using finite temperature QMC [24]. Here, too, no Slater limit in the sense that a finite critical U exists where the gap in the spectrum vanishes can be found. While QMC calculations are typically restricted in the accessible values of Coulomb parameter U and temperature

T , such restrictions do not apply to the NRG. Hence, in particular for finite doping, we expect the NRG to be a rather powerful tool to address the question of possible non Fermi liquid properties as $T \rightarrow 0$.

Summary and conclusions

Since its development in 1998 the DCA has become a tool to systematically study the influence of nonlocal correlations on the physics of correlated electron systems. While one of the major achievements surely was the observation of d -wave superconductivity for the Hubbard model [14], another important aspect is the question, whether for the 2D Hubbard model there exists a parameter regime where non Fermi liquid physics can be observed in the ground state. Certain evidence exists from QMC calculations at finite temperatures within the DCA [20,30], while weak-coupling results suggest the existence of a very small low-energy scale [31]. The final answer whether even in the DCA one might again encounter a Fermi liquid at very low temperatures requires a non-perturbative tool that allows to do calculations close to or at $T = 0$. Such a tool is the NRG, which has already proven its potentials in connection with the DMFT. Here, a first application of this technique to solve the embedded cluster problem of the DCA is presented. Currently, we are restricted to cluster sizes $N_c = 2$, but this is already sufficient to observe generic properties of the Hubbard model, like the formation of a gap *without* long-range magnetic order for arbitrarily small values of U at half filling. Since we believe that the question whether for small doping the system may exhibit Fermi liquid properties at $T = 0$ or not is intimately connected to short-ranged fluctuations, which are captured by the $N_c = 2$ cluster already, we believe that at least a qualitative answer will be possible. Work along these lines is in progress.

We acknowledge useful conversations with H. Monien, R. Bulla, M. Potthoff and D. Vollhardt. This work was supported by NSF grant DMR-0073308 and by the Deutsche Forschungsgemeinschaft through the SFB 484 “Kooperative Phänomene im Festkörper”. Part of this research was performed by TM as a Eugene P. Wigner Fellow and staff member at the Oak Ridge National Laboratory, managed by UT-Battelle, LLC, for the U.S. Department of Energy under Contract DE-AC05-00OR22725. We acknowledge supercomputer support by the Leibniz Rechenzentrum in Munich and the computer center of the Max-Planck society in Garching under grant h0301.

References

1. M. Imada, A. Fujimori, and Y. Tokura, Rev. Mod. Phys. **70**, 1039 (1998).
2. J. Hubbard, Proc. R. Soc. London **A276**, 238(1963); M.C. Gutzwiller, Phys. Rev. Lett. **10**, 59(1963); J. Kanamori, Prog. Theor. Phys. **30**, 275(1963).
3. W. Metzner und D. Vollhardt, Phys. Rev. Lett. **62**, 324(1989).

4. T. Pruschke, M. Jarrell and J.K. Freericks, *Adv. Phys.* **42**, 187 (1995);
5. A. Georges, G. Kotliar, W. Krauth and M.J. Rozenberg, *Rev. Mod. Phys.* **68**, 13(1996).
6. M. Jarrell and Th. Pruschke, *Z. Phys.* **B90**, 187 (1993).
7. P.G.J. van Dongen, *Phys. Rev. Lett.* **67**, 757 (1991); *Phys. Rev.* **B50**, 14016 (1994).
8. R. Zitzler, Th. Pruschke, R. Bulla, *Eur. Phys. J. B* **27**, 473 (2002).
9. Y. Nagaoka, *Phys. Rev.* **147**, 392 (1966).
10. Th. Obermeier, Th. Pruschke and J. Keller, *Phys. Rev.* **B56**, R8479 (1997).
11. D. Vollhardt, N. Blümer, K. Held, M. Kollar, J. Schlipf and M. Ulmke, *Z. Phys.* **B103**, 283(1997); M. Ulmke, *Eur. Phys. J. B1*, 301 (1998).
12. E.H. Lieb and F.Y. Wu, *Phys. Rev. Lett.* **20**, 1445 (1968).
13. M.H. Hettler, A.N. Tahvildar-Zadeh, M. Jarrell, T. Pruschke and H. R. Krishnamurthy, *Phys. Rev. B* **58**, 7475 (1998); M.H. Hettler, M. Mukherjee, M. Jarrell and H. R. Krishnamurthy, *Phys. Rev. B* **61**, 12739 (2000).
14. Th. Maier *et al.*, *Eur. Phys. J. B* **13**, 613 (2000); Th. Maier, M. Jarrell, Th. Pruschke, and J. Keller, *Phys. Rev. Lett.* **85**, 1524 (2000).
15. C. Huscroft, M. Jarrell, Th. Maier, S. Moukouri, and A.N. Tahvildarzadeh, *Phys. Rev. Lett.* **86**, 139 (2001).
16. S. Moukouri and M. Jarrell, to appear in *Computer Simulations in Condensed Matter Physics VII*, Eds. D.P. Landau, K. K. Mon, and H. B. Schuttler (Springer-Verlag, Heidelberg, Berlin, 2000).
17. M. Jarrell, Th. Maier, C. Huscroft, S. Moukouri, *Phys. Rev. B*, to appear, cond-mat/0108140.
18. K.G. Wilson, *Rev. Mod. Phys.* **47**, 773 (1975); H.R. Krishna-murthy, J.W. Wilkins, and K.G. Wilson, *Phys. Rev. B* **21**, 1003 (1980); *ibid.* **21**, 1044 (1980).
19. R. Bulla, *Phys. Rev. Lett.* **83**, 136 (1999); R. Bulla, T.A. Costi, D. Vollhardt *Phys. Rev. B* **64**, 045103 (2001).
20. Th. Pruschke *et al.* in “High Performance Computing in Science and Engineering”, S. Wagner, W. Hanke, A. Bode and F. Durst (eds.), Springer Verlag 2003, p. 327.
21. M. Jarrell, *Phys. Rev. Lett.* **69**, 168 (1992).
22. R. Bulla, A.C. Hewson and Th. Pruschke, *J. Phys.: Condens. Matter* **10**, 8365(1998).
23. The use of OpenMP turned out to be inefficient. A sizeable speedup could only be obtained up to 4 SMP processors; using more processors mainly increased the system time.
24. S. Moukouri and M. Jarrell, *Phys. Rev. Lett.* **87**, 167010 (2001) .
25. T.D. Stanescu and P. Phillips, cond-mat/0301254 (2003).
26. C. Dahnken, M. Aichhorn, W. Hanke, E. Arrigoni, M. Potthoff, cond-mat/0309407 (2003).
27. N. E. Bickers, D. J. Scalapino, S. R. White, *Phys. Rev. Lett.* **62**, 961 (1989).
28. S. Wernbter, *Phys. Rev.* **B55**, 10149 (1997).
29. C. Gröber, R. Eder and W. Hanke, *Phys. Rev.* **B62**, 4336 (2000).
30. Th.A. Maier, Th. Pruschke and M. Jarrell, *Phys. Rev.* **B66**, 075102 (2002).
31. J. Altmann, W. Brenig and A.P. Kampf, *Eur. Phys. J. B18*, 429(2000).
32. Th. Pruschke and R. Zitzler, *J. Phys.: Condens. Matter* **15**, 7867 (2003).